A Novel Back Propagation Neural Network-square Root Cubature Kalman Filtering Strategy Based on Fusion Dual Factor Parameter Identification for State-of-Charge Estimation of Lithium-ion Batteries

Xu, Xuntao; Wang, Shunli; Wang, Chao; Fernandez, Carlos; Blaabjerg, Frede

Published in:
Proceedings of 2024 IEEE 4th New Energy and Energy Storage System Control Summit Forum, NEESSC 2024

DOI (link to publication from Publisher):
10.1109/NEESSC62857.2024.10733526

Publication date:
2024

Document Version
Accepted author manuscript, peer reviewed version

A Novel Back Propagation Neural Network-square Root Cubature Kalman Filtering Strategy Based on Fusion Dual Factor Parameter Identification for State-of-Charge Estimation of Lithium-ion Batteries

Xuntao Xu
School of Electronics and Information
MianYang Polytechnic
Mianyang, China

Shunli Wang*
Electric Power College
Inner Mongolia University of Technology
Hohhot, China
* Corresponding author: wangshunli1985@qq.com

Chao Wang
School of Information Engineering
Southwest University of Science and Technology
Mianyang, China

Carlos Fernandez
School of Pharmacy and Life Sciences
Robert Gordon University
Aberdeen, UK

Frede Blaabjerg
Department of Energy Technology
Aalborg University
Aalborg, Denmark

***Abstract*—Accurate real-time estimation of the state-of-charge (SOC) of the battery is of great significance for promoting the development of electric vehicles. In this research, a novel back propagation neural network-square root cubature Kalman filtering (BPNN-SRCKF) strategy based on fusion dual factor parameter identification for SOC estimation of lithium-ion batteries is proposed. First of all, with the organic integration of the forgetting factor and memory length, a dual factor parameter identification algorithm is designed. Secondly, the square root filtering is incorporated into the CKF algorithm to speed up the operation and avoid filter divergence. Finally, a BPNN is introduced to improve the fault tolerance of the model. The results show that the mean absolute error and root mean square error range from 1.13%~1.28% under complex working conditions, which proves that the proposed strategy has high precision and good robustness.**

Keywords-lithium-ion battery; state-of-charge; dual-factor parameter identification; square root cubature Kalman filtering; back propagation neural network

I. INTRODUCTION

To alleviate the energy crisis, the development of sustainable clean energy has been paid attention to by many developed and developing countries. [1,2]. Lithium-ion batteries (LIB) have been widely used in electric vehicles (EV) due to their large capacity, clean and environmental protection, and so on [3]. SOC is a key state parameter for battery management system (BMS) evaluation, which has an important impact on the battery life and safety of EVs [4]. Therefore, this paper focuses on the estimation strategy of SOC for power LIBs.

At present, SOC estimation methods are mainly divided into three categories: experimental test method, data-driven method, and model-driven method [5]. The experimental test method is suitable for accurate measurement in the laboratory. [6]. The data-driven method refers to establishing the mapping relationship between battery measured data and SOC through machine learning algorithms [7]. El Fallah et al. [8] designed experimental plans to verify the performance of different neural networks in estimating SOC. The results express that deep neural network has good accuracy and robustness. However, the method based on neural networks has high requirements for computing power and data quality.

The equivalent circuit model (ECM) has been widely used due to its simplicity and efficiency, such as Kalman filtering based on ECM [9, 10]. Yun et al. [11] proposed an improved extended Kalman filter (EKF) method, which can estimate SOC more accurately under various simulation conditions. Wu et al [12] proposed a multi-scale fractional order double UKF to realize the joint estimation of parameters and SOC. The results prove that the accuracy and robustness of the proposed method are greatly improved. Given the shortcomings of EKF and UKF, Zhuang et al. [13] employ the cubature Kalman filter (CKF) algorithm to estimate SOC. The results show that the optimized CKF greatly improves the algorithm accuracy.

To sum up, traditional methods are more flexible and mature, while data-driven methods are more complex and costly to apply at present. Therefore, a novel BPNN-SRCKF strategy based on fusion dual factor parameter identification for SOC estimation is proposed. To overcome the defects of traditional parameter identification, a least squares algorithm combining the forgetting factor and memory length is designed. To improve the estimation performance of SOC, SR filtering and BPNN are introduced to optimize CKF.

II. FUSION DUAL FACTOR PARAMETER IDENTIFICATION

A. Second-order Modeling and State Space Equation

In this article, the second-order equivalent circuit model (SO-ECM) is adopted in this study, as shown in Fig. 1.

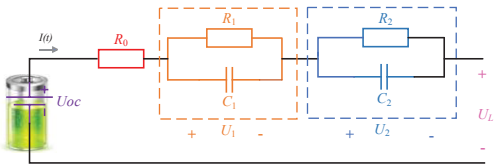

Figure 1. SO-ECM of lithium-ion batteries.

In Fig. 1, U_{OC} and U_L represent the OCV and measuring terminal voltage. R_0 represents the internal ohmic resistance, R_1 and R_2 represent the polarization resistance, and C_1 and C_2 represent the polarization capacitance. Assuming the current I is the positive direction during discharge, the voltage and current expression as shown in Eq. (1).

$$\begin{cases} U_L = U_{OC} - IR_0 - U_1 - U_2 \\ \dfrac{dU_1}{dt} = \dfrac{I}{C_1} - \dfrac{U_1}{R_1C_1} \\ \dfrac{dU_2}{dt} = \dfrac{I}{C_2} - \dfrac{U_2}{R_2C_2} \end{cases} \tag{1}$$

A functional relationship between U_{OC} and SOC can be established from the OCV-SOC fitting curve. $x = [SOC, U_1, U_2]^T$ is selected as the state variable, and Eq. (1) is discretized, as shown in Eq. (2)

$$\begin{cases} \begin{bmatrix} SOC_{k+1} \\ U_{1,k+1} \\ U_{2,k+1} \end{bmatrix} = \begin{bmatrix} 1 & 0 & 0 \\ 0 & e^{-\frac{\Delta t}{\tau_1}} & 0 \\ 0 & 0 & e^{-\frac{\Delta t}{\tau_2}} \end{bmatrix} \begin{bmatrix} SOC_k \\ U_{1,k} \\ U_{2,k} \end{bmatrix} + \begin{bmatrix} -\dfrac{\eta \Delta t}{Q_N} \\ R_1\left(1 - e^{-\frac{\Delta t}{\tau_1}}\right) \\ R_2\left(1 - e^{-\frac{\Delta t}{\tau_2}}\right) \end{bmatrix} I_k + w_k \\ U_{L,k+1} = U_{OC,k+1} - U_{1,k+1} - U_{2,k+1} - IR_0 + v_k \end{cases} \tag{2}$$

In Eq. (2), Δt said sampling time interval, τ as the time constant, $\tau_1 = R_1C_1$, $\tau_2 = R_2C_2$. w_k and v_k are system state noise and measurement noise respectively. Q_0 means the capacity of the battery, η for coulomb efficiency.

B. FF-LMRLS Algorithm

The general form of RLS is shown in Eq. (3).

$$y(k) = \phi(k)^{\mathrm{T}} \theta(k) + e(k) \tag{3}$$

In Eq. (3), y(k), $\phi(k)$, θ(k) and e(k) indicate the output of the system, the observation value, the parameter to be estimated and the noise observation value.

As the number of recursions and the amount of data increases, the RLS algorithm will appear data saturation phenomenon [14]. The limited memory least square (LMRLS) method improves the calculation speed and alleviate the phenomenon of data saturation [10, 15]. In this study, the forgetting factor-limited memory least square (FF-LMRLS) algorithm is designed. Compared with RLS, FF-LMRLS takes into account the advantages of forgetting factor recursive least square (FFRLS) and LMRLS, which can effectively remove the redundancy of invalid data and improve calculation speed and accuracy. Let the forgetting factor of the FF-LMRLS algorithm be λ, the memory length be L, and its recursive flow is as follows.

Step 1: Calculate the parameter estimate of memory length L

$$\begin{cases} \hat{\theta}(k+1) = \hat{\theta}(k) + K(k+1)[y(k+1) - \phi^T(k+1)\hat{\theta}(k)] \\ K(k+1) = P(k+1)\phi(k+1)[\phi^T(k+1)P(k)\phi(k+1) + \lambda]^{-1} \\ P(k+1) = [H - K(k+1)\phi^T(k+1)]P(k) \end{cases} \tag{4}$$

Step 2: Calculate the parameter estimate of length L+1 at time k

$$\begin{cases} \hat{\theta}(k-L,k) = \hat{\theta}(k-L,k-1) + K(k-L,k)[y(k) - \phi^T(\mathrm{k})\hat{\theta}(k-L,k-1)] \\ K(k-L,k) = P(k-L,k-1)\phi(k)[\phi^T(\mathrm{k})P(k-L,k-1)\phi(k) + \lambda]^{-1} \\ P(k-L,k) = [H - K(k-L,k)\phi^T(k)]P(k-L,k-1) \end{cases} \tag{5}$$

Step 3: Calculate the parameter estimate of length L at time k

$$\begin{cases} \hat{\theta}(k-L+1,k) = \hat{\theta}(k-L,k) - K(k-L+1,k)[y(k-L) - \phi^T(k-L)\hat{\theta}(k-L,k)] \\ K(k-L+1,k) = P(k-L,k)\phi(k-L)[\phi^T(k-L)P(k-L,k)\phi(k-L) + \lambda]^{-1} \\ P(k-L+1,k) = [H + K(k-L+1,k)\phi^T(k-L)]P(k-L,k) \end{cases} \tag{6}$$

Where, K (*) and P (*) indicate the gain function and covariance function respectively. H indicates the unit matrix. The principle flow chart of FF-LMRLS is shown in Fig. 2.

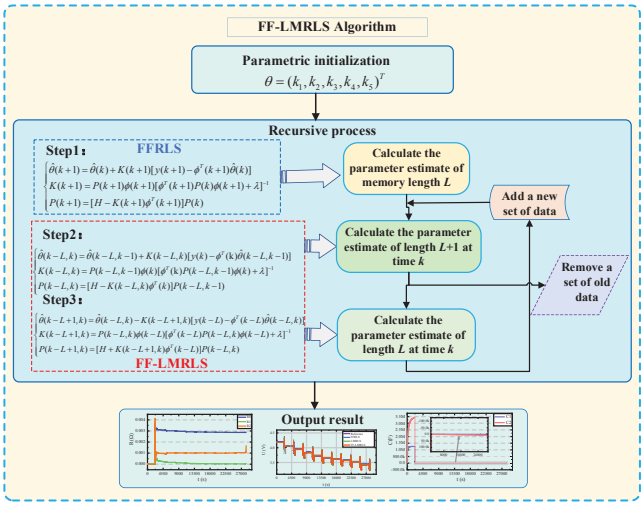

Figure 2. Flowchart of the FF-LMRLS.

As shown in Fig. 2, first, the parameters to be identified are initialized. And then the FF-LMRLS recursive operation is performed, which will prepare for the SOC estimation in the next step.

III. BPNN-SRCKF ALGORITHM MODEL

The CKF has less computation than the UKF and its calculation accuracy is higher than that of EKF [16, 17]. The SR filtering directly updates recursively in the form of the square root of the covariance matrix, which not only reduces computational complexity but also avoids filter divergence [18]. Therefore, this paper uses SRCKF to estimate SOC. The neural network has a strong nonlinear processing ability and self-learning ability, especially suitable for dealing with non-linear lithium battery systems [19, 20]. BPNN is a simple and effective network. To improve the nonlinear processing capability and fault tolerance of the estimation model, the BPNN is introduced. Therefore, a BPNN-SRCKF algorithm model is established in this study. The detailed steps are as follows.

Step 1: Parameter initialization

The state variable $\hat{x}_k$ and error covariance P_k are initialized to obtain $\hat{x}_{0|0}$, $P_{0|0}$. *Q and R represent the process noise and measurement noise respectively*.

Step 2: Time update

1) Cubature point calculation

$$x_{i,k-1|k-1}=S_{k-1|k-1}\xi_i+\hat{x}_{k-1|k-1} \tag{7}$$

In Eq. (7), $x_{i,k-1|k-1}$ is the *i*th cubature point at time *k*-1, i = 1 ,2 ,3, …, m, m=2n determines the number of cubature points, n represents the dimension of the state variable, ξ_j is the cubature point set.

2) Cubature point propagation

$$\hat{x}^*_{i,k|k-1}=f(x_{i,k-1|k-1},u_k) \tag{8}$$

In Eq. (8), $\hat{x}^*_{i,k|k-1}$ represents the *i*th propagated cubature point at time *k*.

3) State prediction value calculation

$$\hat{x}_{k|k-1}=\frac{1}{2n}\sum_{i=1}^{2n}\hat{x}^*_{i,k|k-1} \tag{9}$$

In Eq. (9), $\hat{x}_{k|k-1}$ represents the state estimate at time *k*

4) Calculation of the SR of the error covariance matrix

$$S_{k|k-1}=Tria\left(\left[\hat{x}^*_{k|k-1},S_{Q,k-1}\right]\right) \tag{10}$$

In Eq. (10), $S_{k|k-1}$ is the SR of the error covariance matrix at time *k*.

$$\begin{cases}\hat{x}^*_{k|k-1}=1/\sqrt{2n}\left[\hat{x}^*_{1,k|k-1}-\hat{x}_{k|k-1}\quad \hat{x}^*_{2,k|k-1}-\hat{x}_{k|k-1}\quad \cdots\quad \hat{x}^*_{2n,k|k-1}-\hat{x}_{k|k-1}\right]\\ S_Q=chol(Q)\end{cases} \tag{11}$$

Step 3: Measurement updates

1) Cubature point calculation

$$x_{i,k|k-1}=S_{k|k-1}\xi_i+\hat{x}_{k|k-1} \tag{12}$$

2) Cubature point propagation

$$Z_{i,k|k-1}=h(x_{i,k|k-1},u_k) \tag{13}$$

In Eq (13), $Z_{i,k|k-1}$ represents the measurement prediction value of the *i*th propagated cubature point.

3) Measurement prediction value calculation

$$\hat{z}_{k|k-1}=\frac{1}{2n}\sum_{i=1}^{2n}Z_{i,k|k-1} \tag{14}$$

4) Calculate the SR of the covariance of the measurement error

$$S_{zz,k|k-1}=Tria\left(\left[\zeta_{k|k-1},S_{R,k}\right]\right) \tag{15}$$

In Eq (15), $\zeta_{k|k-1}$, $S_{R,k}$ as shown in the following.

$$\begin{cases}\zeta_{k|k-1}=1/\sqrt{2n}\left[Z_{1,k|k-1}-\hat{z}_{k|k-1}\quad Z_{2,k|k-1}-\hat{z}_{k|k-1}\quad \cdots\quad Z_{2n,k|k-1}-\hat{z}_{k|k-1}\right]\\ S_R=chol(R)\end{cases} \tag{16}$$

5) Calculate the covariance between the state prediction value and the measurement prediction value

$$P_{xz,k|k-1} = x_{k|k-1}\zeta_{k|k-1}^{T} \tag{17}$$

Step 4: State estimation

1) Kalman gain calculation

$$K_k = (P_{xz,k|k-1} / S_{zz,k|k-1}^{T}) / S_{zz,k|k-1} \tag{18}$$

2) State estimate calculation

$$\hat{x}_{k|k} = \hat{x}_{k|k-1} + K_k\left(z_k - \hat{z}_{k|k-1}\right) \tag{19}$$

3) Calculate the SR estimate of the error covariance

$$S_{k|k} = Tria\left(\left[x_{k|k-1} - K_k\zeta_{k|k-1}, K_k S_{R,k}\right]\right) \tag{20}$$

Step 5: BPNN modify SRCKF

$$SOC_{BPNN-SRCKF}(k) = SOC_{SRCKF}(k) + Err'(k) \tag{21}$$

In Eq. (21), $SOC_{BPNN\text{-}SRCKF}$ represents the SOC estimate after BPNN optimization, SOC_{SRCKF} represents the SOC estimate of the SRCKF algorithm, and *Err'* is the corrected error function obtained by BPNN training. The BPNN-SRCKF algorithm model flow chart is shown in Fig. 3.

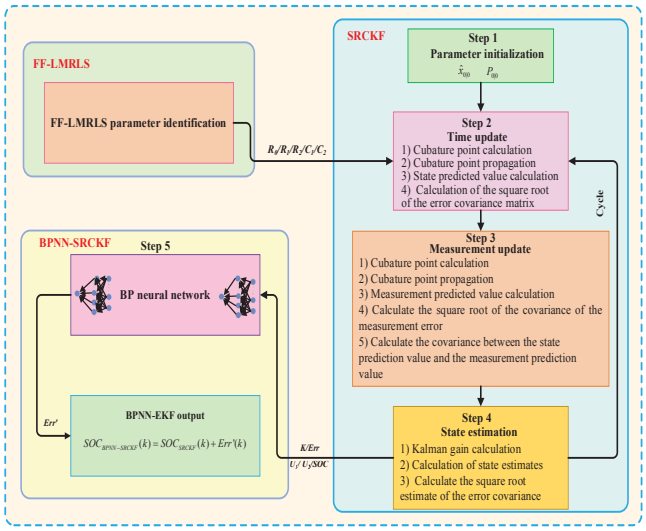

Figure 3. The BPNN-SRCKF model flow chart.

In Fig. 3, the whole SOC estimation process consists of three modules: the FF- LMRLS online parameter identification module, the SRCKF online state estimation module, and the BPNN error correction module.

IV. EXPERIMENTAL VERIFICATION

A. Experimental Platform Construction

The battery capacity in this study is 45Ah. The experimental platform consists of a charge/discharge tester, a thermostat, and a computer, as shown in Fig. 4.

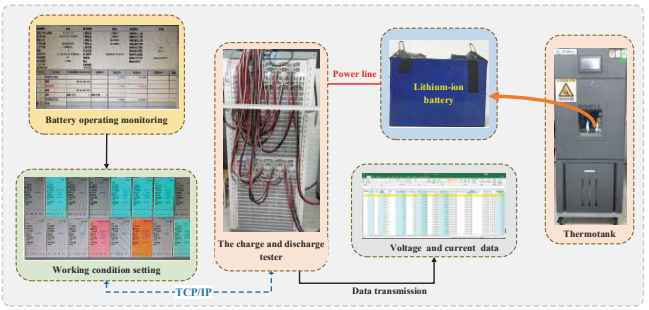

Figure 4. Experimental test platform.

The experimental working conditions of this study include the hybrid pulse power characterization (HPPC) test, dynamic stress test (DST), and Beijing bus dynamic stress test (BBDST). The experimental procedures for HPPC, DST, and BBDST working conditions can be found in the literature [10].

B. Verification of Fusion Dual Factor Parameter Identification

The parameter identification and verification results are shown in Fig. 5.

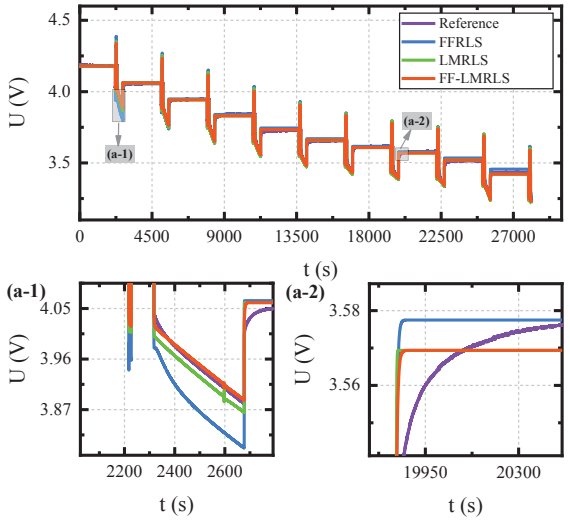

Figure 5. Voltage simulation results under HPPC.

From Fig. 5, it can be seen that the FF-LMRLS algorithm can well follow the reference voltage curve. This shows that the organic combination of limited memory L and forgetting factor λ further improves the tracking performance of least squares. The evaluation metrics of this study are represented by the maximum error (MAXE), the mean absolute error (MAE), and the root mean square error (RMSE).

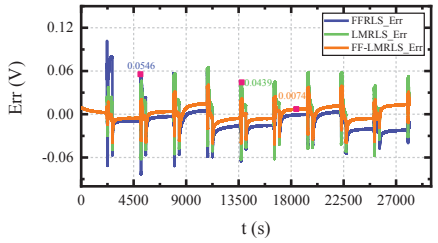

(a) Error comparison

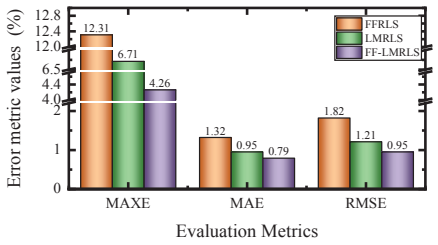

(b) Error evaluation metrics

Figure 6. Simulation voltage error and error metrics.

From Fig. 6 (a), it can be seen that the error curve of the FF-LMRLS algorithm fluctuates less than that of the FFRLS and FF-LMRLS at the beginning and end phases of the experiment. Further analysis from the Fig. 6 (b) shows that the MAXE of FF-LMRELS is reduced by 8.05% compared to FFRLS, and its MAE and RMSE are 0.79% and 0.95%, respectively, indicating that the FF-LMRELS has high accuracy and robustness.

C. *Verification of BPNN-SRCKF Algorithm Model*

The verification scheme of this study is as follows. First, the HPPC, DST and BBDST operating data required by the experiment are obtained. Then BPNN is trained with DST data. Finally, HPPC and BBDST data are used for verification.

1) Verification under HPPC working condition

The initial value of SOC estimation is set to 1, and the verification results are shown in Fig. 7.

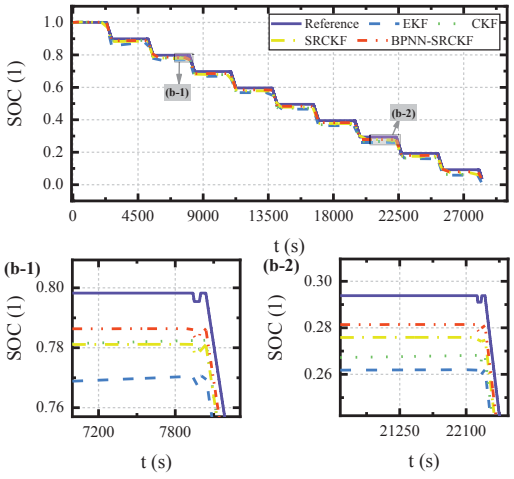

Figure 7. SOC estimation results under HPPC working condition.

In Fig. 7, we can see that the SOC estimated by the BPNN-SRCKF can follow the reference SOC better. Followed by SRCKF, CKF and EKF. It can be seen that the SR and BPNN optimization strategies introduced in this study can improve the SOC estimation performance.

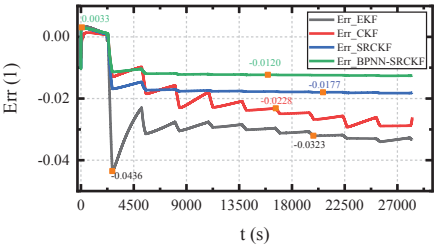

(a) Error of SOC estimation

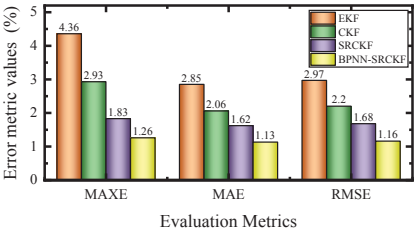

(b) Error evaluation metrics of SOC estimation

Figure 8. Error of SOC estimation under HPPC.

From Fig. 8 (a), it can be seen that the BPNN-SRCKF has the best overall convergence. In the comparison of the CKF and SRCKF algorithms, it can be seen that the convergence rate of SRCKF is fast, which indicates that SR can improve the convergence performance of CKF. Further analysis from Fig. 8 (b), it can be seen that the method proposed in this study can effectively improve the estimation accuracy of SOC. The MAXE, MAE, and RMSE of the BPNN-SRCKF are 1.26%, 1.13%, and 1.16% respectively. It denotes that the algorithm proposed in this study has high accuracy and robustness.

1) Verification under BBDST working condition

The initial value of SOC estimation is set to 1. The verification results are shown in Fig. 9.

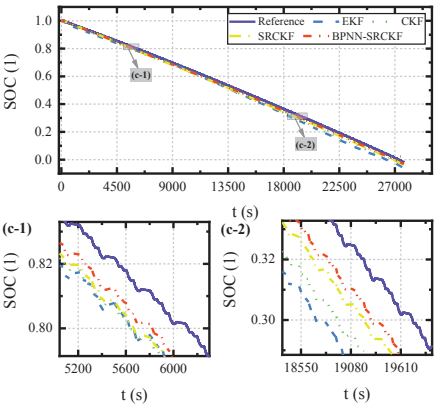

Figure 9. SOC estimation results under BBDST

From Fig. 9, it can be seen that the BPNN-SRCKF algorithm has better tracking performance. It proves that the proposed method can effectively improve the following ability of the algorithm.

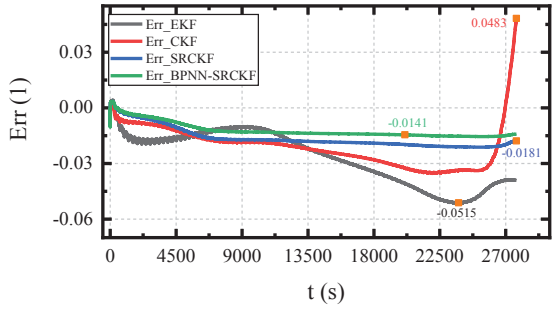

(a) Error of SOC estimation

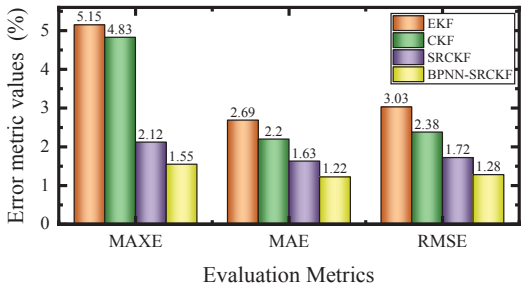

(b) Error evaluation metrics of SOC estimation

Figure 10. Error of SOC estimation under BBDST

From Fig. 10 (a), the SRCKF and BPNN-SRCKF have better convergence. From Fig. 10 (b), the MAXE of SRCKF is about half lower than that of EKF and CKF, indicating that SR improves the filtering stability. The MAE and RMSE of BPNN-SRCKF are reduced by 0.98% and 1.1% respectively compared with CKF, indicating that BPNN further improves the estimation accuracy and robustness.

3) Verification under different SOC initial values

To further analyze the adaptive adjustment capability of the BPNN-SRCKF estimation model, the initial SOC value is set as 0.8 under HPPC working condition. The experimental results are shown in Fig. 11.

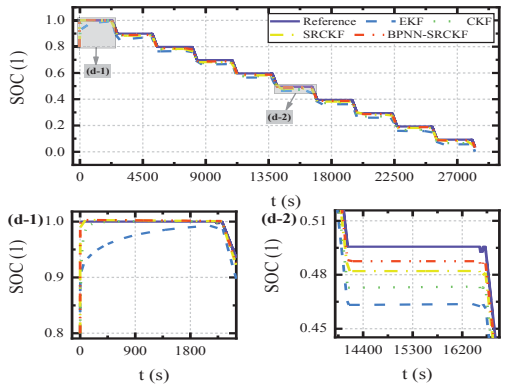

Figure 11. SOC estimation results when the initial value is 0.8.

As can be seen from Fig. 11, when the initial value of SOC has a large deviation from the true value, the BPNN-SRCKF can quickly correct to the exact value and maintain a relatively high tracking accuracy. It shows that the proposed method has fast convergence speed and high accuracy.

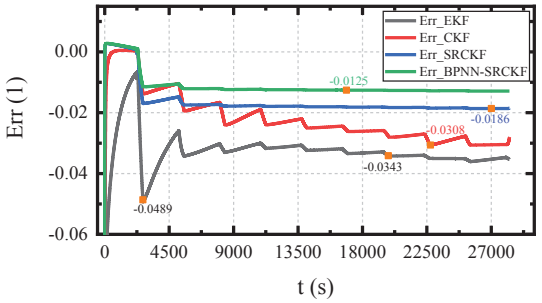

(a) Error of SOC estimation

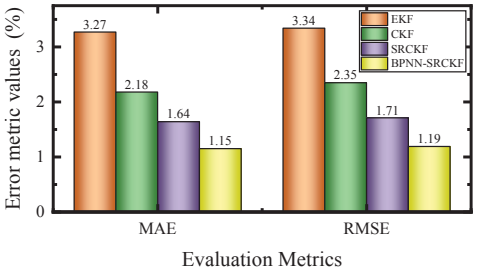

(b) Error evaluation metrics of SOC estimation

Figure 12. Error comparison when the initial value is 0.8.

It can be further seen from Fig. 12 that even if the SOC initial value deviation is large, the convergence and accuracy of SRCKF and BPNN-SRCKF are still not affected. The RMSE and MAE of BPNN-SRCKF are 1.19% and 1.15%, which is not much different from when the SOC initial value is 1. It shows that the model proposed in this study has strong calibration ability and robustness.

V. CONCLUSIONS

Accurate SOC estimation is of great significance to the application and development of lithium batteries. To achieve an accurate and reliable online estimation of SOC, this study established a BPNN-SRCKF estimation model based on fused dual-factor parameter identification. The results show that the MAE and RMSE of FF-LMRLS are 0.79% and 0.95% respectively, indicating that this algorithm can effectively improve the accuracy and stability of the least squares algorithm. To improve the estimation accuracy of SOC, this study introduces SR and BPNN to improve the convergence and adaptability of CKF. Experimental results show that the MAE and RMSE of BPNN-SRCKF under complex working conditions are between 1.13% and 1.28%, which shows that the method proposed in this study can effectively improve the precision and stability of SOC estimation. This will provide a reference for the improvement of the real-time monitoring performance of the BMS, then further improve the safety performance of EVs.

ACKNOWLEDGMENT

The work is supported by the National Natural Science Foundation of China (No. 62173281), Sichuan Science and Technology Program (No. 24NSFSC0024), Dazhou City School Cooperation Project (No. DZXQHZ006), Technopole Talent Summit Project (No. KJCRCFH08), and Robert Gordon University.

REFERENCES

[1] C. N. Zou, et al., "Earth energy evolution, human development and carbon neutral strategy," Petroleum Exploration and Development, vol. 49, no.2, pp. 468-488, 2022.

[2] F. Kong, "A better understanding of the role of new energy and green finance to help achieve carbon neutrality goals, with special reference to China," Science Progress, vol.105, no.1, pp: 1-23, 2022.

[3] J. L. Qiao, et al., "A chaotic firefly- Particle filtering method of dynamic migration modeling for the state-of-charge and state-of-health co-estimation of a lithium-ion battery performance," Energy, vol. 263, pp. 1-11, 2023.

[4] Y. F. Liu, et al., "A review of lithium-ion battery state of charge estimation based on deep learning: Directions for improvement and future trends," Journal of Energy Storage, vol. 52, pp. 1-15, 2022.

[5] L.Zhou, et al., "State estimation models of lithium-ion batteries for battery management system: status, challenges, and future trends," Batteries-Basel, vol. 9, no.2, pp. 1-23, 2023.

[6] M. Adaikkappan and N. Sathiyamoorthy, "Modeling, state of charge estimation, and charging of lithium-ion battery in electric vehicle: A review," International Journal of Energy Research, vol. 46, no.3, pp. 2141-2165, 2022.

[7] M. Kurucan, et al., "Applications of artificial neural network based battery management systems: A literature review," Renewable & Sustainable Energy Reviews, vol. 192, pp. 1-18, 2024.

[8] S. El Fallah, et al., "State of charge estimation of an electric vehicle's battery using Deep Neural Networks: Simulation and experimental results," Journal of Energy Storage, vol. 62, pp. 1-16, 2023.

[9] W. L. Zhou, et al., "Review on the battery model and SOC estimation method," Processes, vol. 9, no.9, pp.1-23, 2021.

[10] C. Wang, et al., "A novel back propagation neural network-dual extended Kalman filter method for state-of-charge and state-of-health co-estimation of lithium-ion batteries based on limited memory least square algorithm," Journal of Energy Storage, vol. 59, pp. 1-13, 2023.

[11] J.J. Yun, et al., "State-of-charge estimation method for lithium-ion batteries using extended kalman filter with adaptive battery parameters," IEEE Access, vol. 11, pp. 90901-90915, 2023.

[12] J.J. Wu, et al., "A multi-scale fractional-order dual unscented Kalman filter based parameter and state of charge joint estimation method of lithium-ion battery," Journal of Energy Storage, vol. 50, pp. 1-14, 2022.

[13] S.Q. Zhuang, et al., "Research on estimation of state of charge of li-ion battery based on cubature kalman filter," Journal of the Electrochemical Society, vol. 169, no.10, pp. 1-9, 2022.

[14] R. H. Guo and W. X. Shen, "An information analysis based online parameter identification method for lithium-ion batteries in electric vehicles," IEEE Transactions on Industrial Electronics, pp. 1-11, 2023.

[15] X.Y. Kong, et al., "Online smart meter measurement error estimation based on EKF and LMRLS method. IEEE Transactions on Smart Grid, vol. 12, no.5, pp. 4269-4279, 2021.

[16] M. Hossain, M. E. Haque and M. T. Arif, "Kalman filtering techniques for the online model parameters and state of charge estimation of the Li-ion batteries: A comparative analysis," Journal of Energy Storage, vol.51, pp. 1-24, 2022.

[17] W. T. Ma, et al., "Robust state of charge estimation for Li-ion batteries based on cubature kalman filter with generalized maximum correntropy criterion," Energy, vol. 260, pp. 1-14, 2022.

[18] M. Y. Zhang, et al., "Improved backward smoothing-square root cubature kalman filtering and variable forgetting factor-recursive least square modeling methods for the high-precision state of charge estimation of lithium-ion batteries," Journal of the Electrochemical Society, vol.170, no. 3, pp. 1-9, 2023.

[19] X. J. Mao, S. J. Song and F. Ding, "Optimal BP neural network algorithm for state of charge estimation of lithium-ion battery using PSO with Levy flight," Journal of Energy Storage, vol.49, pp. 1-5, 2022.

[20] S. L. Wang, et al., "Improved anti-noise adaptive long short-term memory neural network modeling for the robust remaining useful life prediction of lithium-ion batteries," Reliability Engineering & System Safety, vol. 230, pp. 1-12, 2023.